Graphical Abstract

Syntheses, crystal structures and density functional theoretical investigations of copper(II) complexes bearing tridentate Schiff base ligands derived from 8-aminoquinoline

Prasanta Kumar Bhaumik, Antonio Bauzá, Antonio Frontera, Shouvik Chattopadhyay
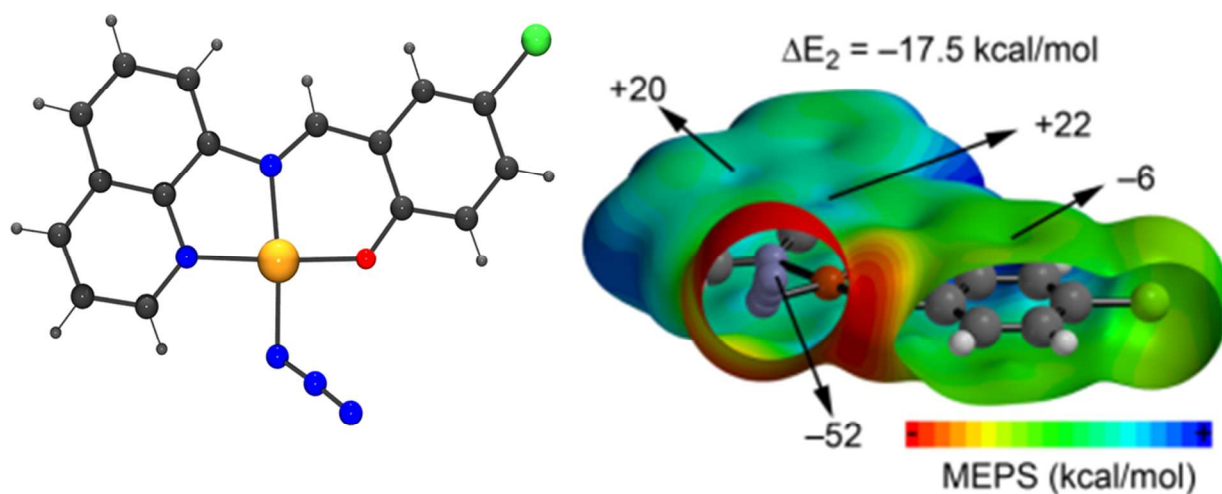
Three copper(II) Schiff base complexes have been synthesized and characterized. The theoretical study, carried out using density functional theory calculations, is devoted to the analysis of the interesting supramolecular assemblies in the solid state of the structures, paying special attention to lp−π and π−π interactions.

Journal Name

ARTICLE

Syntheses, crystal structures and density functional theoretical investigations of copper(II) complexes bearing tridentate Schiff base ligands derived from 8-aminoquinoline

Prasanta Kumar Bhaumik,[a] Antonio Bauzá,[b] Antonio Frontera,*[,b] Shouvik Chattopadhyay*[,a]

Three copper(II) complexes, *[Cu(L^1)(H$_2$O)(OClO$_3$)]$_n$* (**1**), *[Cu(L^1)(N$_3$)]* (**2**) and *[Cu(L^2)(Cl)(H$_2$O)]* (**3**) *HL^1* = 4-chloro-2-((quinolin-8-ylimino)methyl)phenol and *HL^2* = 2-ethoxy-6-((quinolin-8-ylimino)methyl)phenol, have been synthesized and characterized by elemental analyses, IR and UV–Vis spectroscopy and single-crystal X-ray diffraction studies. The theoretical study, carried out using density functional theory (DFT) calculations, is devoted to the analysis of the interesting supramolecular assemblies in the solid state of the structures, paying especial attention to lp–π and π–π interactions involving the quinolin-8-ylimino moiety.

1.Introduction

The non-covalent interactions, popularly known as "supramolecular interactions", have shown to play an important role in structural biology and supramolecular chemistry.[1-6] The synchronization of many chemical and biological processes is often executed by combinations of different non-covalent interactions.[7] The correct description of these non-covalent interactions is needed for the understanding and development of supramolecular chemistry. A number of well-recognized strong, directional non-covalent interactions such as hydrogen bonding and halogen bonding, and less directional forces like ion pairing have been used to govern the organization of multi-component supramolecular assemblies.[8-11] In addition, non-covalent interactions involving aromatic rings {π-π stacking, cation-π, C–H/π, lp-π and anion-π interactions}[12-16] are enormously significant in this field. They could play a key role in chemistry and biology, in particular, drug–receptor interactions, crystal engineering, enzyme inhibition and protein folding.[17] They could also manage the structures of bio-molecules e.g. proteins and DNA, several host–guest systems, enzyme–substrate binding etc.[18-19] They have also shown to have the ability to regulate antigen–antibody recognition.[20-21] Because of their ubiquitous role in diverse fields, the investigation and understanding of these weak non-covalent interactions have become one of the major objectives of contemporary chemistry.

Consequently, the relevance of these non-covalent interactions is broadly analysed by a large number of researchers using combined theoretical and experimental investigations[22-28] and currently it is an interesting topic of research.

In the present work, we have used two Schiff bases, *HL^1* = 4-chloro-2-((quinolin-8-ylimino)methyl)phenol and *HL^2* = 2-ethoxy-6-((quinolin-8-ylimino)methyl)phenol to prepare three copper(II) complexes, *[Cu(L^1)(H$_2$O)(OClO$_3$)]$_n$*(**1**), *[Cu(L^1)(N$_3$)]* (**2**) and *[Cu(L^2)(Cl)(H$_2$O)]* (**3**). The structures of all three complexes have been characterized by single crystal X-ray crystallography. Three complexes presented interesting supramolecular assemblies in the solid state dominated by H-bonding, π-π and lp-π interactions that are analyzed in detail by means of DFT calculations allowing the calculation of the different contributions to the molecular recognition.

2. Experimental

2.1. Materials

All chemicals were of AR grade and were used as purchased from Sigma-Aldrich without further purification.
Caution!!
Complexes containing azide and perchlorate are potentially explosive. Only small amount of those materials should be prepared and handled with care.

2.2. Preparations

2.2.1. Preparation of ligands, *HL¹* and *HL²*

The tridentate Schiff bases, *HL¹* {4-chloro-2-((quinolin-8-ylimino)methyl)phenol} and *HL²* {2-ethoxy-6-((quinolin-8-ylimino)methyl)phenol} were synthesized by refluxing quinolin-8-amine (144 mg, 1 mmol), respectively with 5-chloro-2-hydroxybenzaldehyde (156.5 mg, 1 mmol) and 3-ethoxy-2-hydroxybenzaldehyde (166 mg, 1 mmol) in methanol (20 ml) for 1 h. The ligands were not isolated and used directly for the preparation of complexes. Structures of ligands are given in Scheme1.
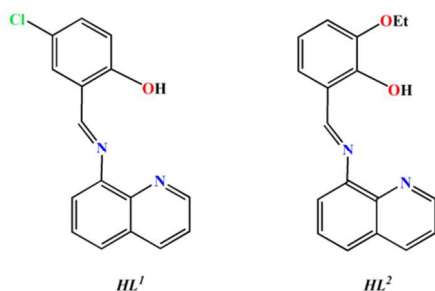
Scheme 1: Schematic representation of ligands used in the present work.

2.2.2. Synthesis of *[Cu(L¹)(H₂O)(OClO₃)]ₙ* (1)

A methanol solution (25 ml) of copper(II) perchlorate hexahydrate (370 mg, 1 mmol) was added to the methanol solution of *HL¹* and the resulting solution was refluxed for 1 h to give a brown solution. It was cooled and kept for a few days to get greenish brown crystalline precipitate. The precipitate was collected by filtration and dissolved in acetonitrile. Single crystals, suitable for X-ray diffraction, were obtained after five days on slow evaporation of the acetonitrile solution in open atmosphere.

Yield: 320 mg (69%). Anal. Calc. for $C_{16}H_{12}Cl_2CuN_2O_6$ (FW 462.73): C, 41.53; H, 2.61; N, 6.05%. Found: C, 41.2; H, 2.3; N, 6.3%. IR (KBr, cm⁻¹): 1612 ($\nu_{C=N}$), 1120 (ν_{ClO4}), 3422 (ν_{OH}), UV–Vis, λ_{max} (nm) (ε_{max}, (L mol⁻¹ cm⁻¹)) (acetonitrile): 619 (1.1 ×10²), 452 (1.1 × 10⁴), 317 (1.4 × 10⁴). Magnetic moment: 1.70 BM.

2.2.3. Synthesis of *[Cu(L¹)(N₃)]* (2)

A methanol solution (25 ml) of copper(II) perchlorate hexahydrate (370 mg, 1 mmol) was added to the methanol solution of *HL¹* and the resulting solution was refluxed for 1 h to give a brown solution. An aqueous methanol solution of sodium azide (65 mg, 1 mmol) was added to it and refluxed again for an additional hour to obtain a brown solution. Thereafter it was cooled to room temperature and an immediate separation of a small amount of side product was filtered off. Single crystals, suitable for X-ray diffraction, were obtained after three days by slow evaporation of the filtrate in open atmosphere.

Yield: 265 mg (68%). Anal. Calc. for $C_{16}H_{10}ClCuN_5O$ (FW 387.29): C, 49.62; H, 2.60; N, 18.08%. Found: C, 49.2; H, 2.8; N, 18.2%. IR (KBr, cm⁻¹):1611 ($\nu_{C=N}$), 2049 (ν_{N3}), 3445 (ν_{OH}), UV–Vis, λ_{max} (nm) (ε_{max}, (L mol⁻¹ cm⁻¹)) (acetonitrile): 613 (1.1

× 10²), 452 (5.6 × 10³), 320 (1.0 × 10⁴). Magnetic moment: 1.72 BM.

2.2.4. Synthesis of *[Cu(L²)(Cl)(H₂O)]* (3)

A methanol solution (25 ml) of copper(II) chloride dihydrate (170 mg, 1 mmol) was added to the methanol solution of *HL²*and the resulting solution was refluxed for 1 h to give a deep brown solution. It was cooled and kept for a few days to get brown precipitate. The precipitate was collected by filtration and dissolved in water and refluxed. It was then cooled to room temperature Single crystals, suitable for X-ray diffraction, were obtained after ten days by slow evaporation of the filtrate in open atmosphere.

Yield: 310 mg (76%). Anal.Calcd.for $C_{18}H_{16}ClCuN_2O_3$ (FW 407.33): C, 53.08; H, 3.96; N, 6.88%. Found: C, 52.8; H, 4.1; N, 7.2%. IR (KBr, cm⁻¹):1607 ($\nu_{C=N}$), 3443 (ν_{OH}), UV–Vis, λ_{max} (nm) (ε_{max}, (L mol⁻¹ cm⁻¹)) (acetonitrile): 603 (1.3 × 10²), 456 (2.4 × 10³), 350 (6.4 × 10³). Magnetic moment: 1.73 BM.

2.3. Physical measurements

Elemental analyses (carbon, hydrogen and nitrogen) were performed using a Perkin–Elmer 240C elemental analyzer. Infrared spectra in KBr (4500–500 cm⁻¹) were recorded using a PerkinElmer FT-IR spectrum two spectrometer. Electronic spectra of complexes **1-3** (in acetonitrile) in the range of 900-200 nm were recorded on a Jasco V-630 UV–Vis spectrophotometer at room temperature (32°C). The magnetic susceptibility measurements were done for complexes **1-3** with an EG and PAR vibrating sample magnetometer, model 155 at room temperature (300 K) in 5000 G magnetic field and diamagnetic corrections were done using Pascal's constants.[29] Effective magnetic moments were calculated using the formula $\mu_{eff} = 2.828(\chi_M T)^{1/2}$, where χ_M is the corrected molar susceptibility.

2.4. X-ray Crystallography

Single crystal of complex **1** was used for data collection using an 'Oxford Diffraction X-Calibur System' diffractometer equipped with graphite-monochromated Mo Kα radiation (λ = 0.71073 Å) at 150 K. Single crystals of complexes **2** and **3** having suitable dimensions, were used for data collection using a 'Bruker SMART APEX II' diffractometer equipped with graphite-monochromated Mo Kα radiation (λ = 0.71073 Å) at 293 K. The R value of **1** was rather high because of the poor quality of the crystals. The poor quality of crystals of **1** gave rise to misshapen large spots in the diffraction pattern which in turn led to several warning signs flagged up by checkcif.

For all three complexes molecular structures were solved by direct methods and refinement by full-matrix least squares on F² using the SHELX-97 package.[30] Non-hydrogen atoms were refined with anisotropic thermal parameters. H atoms, attached with O atom, were located by different Fourier maps and were kept fixed. All other H atoms were placed in their geometrically idealized positions and constrained to ride on their parent atoms. Empirical absorption corrections were applied to **1** using the ABSPACK program.[30] Multi-scan empirical absorption

corrections were applied to **2** and **3** using the program SADABS.[31]

2.5. Theoretical methods

The geometries of the complexes included in this study were computed at the BP86-D3/def2-TZVP level of theory using the crystallographic coordinates within the TURBOMOLE program.[32] This level of theory that includes the latest available dispersion correction (D3) is adequate for studying non covalent interactions dominated by dispersion effects like π-stacking. The basis set superposition error for the calculation of interaction energies has been corrected using the counterpoise method.[33] The "atoms-in-molecules" (AIM)[34] analysis of the electron density has been performed at the same level of theory using the AIMAll program.[35]

3. Results and discussion

3.1. Syntheses

The Schiff base ligands, HL^1 and HL^2 are produced by the 1:1 condensation of quinolin-8-amine respectively with 5-chloro-2-hydroxybenzaldehyde and 3-ethoxy-2-hydroxybenzaldehyde in methanol following the literature method.[36] A methanol solution of HL^1 was made to react with copper(II) perchlorate hexahydrate to prepare the complex **1**, $[Cu(L^1)(H_2O)(OClO_3)]_n$, which on refluxing with sodium azide produced complex **2**, $[Cu(L^1)(N_3)]$. Similarly on reaction of a methanol of HL^2 with copper(II) chloride dihydrate produced complex **3**.

3.2. IR, electronic spectra and magnetic moments

The IR bands corresponding to the C=N stretching vibrations for complexes **1-3** appear in the range 1607–1650 cm^{-1}.[37] A broad band at around 1120 cm^{-1} in the IR spectrum of complex **1** indicates the presence of perchlorate anion.[38] The IR spectrum of complex **2** exhibits characteristic ν_{N3} band at 2049 cm^{-1}.[39] In IR spectra of complexes **1** and **3**, broad bands at 3422 and 3443 cm^{-1} respectively were observed, which may be assigned to the OH stretching vibration of coordinated water molecules.

The electronic spectra in acetonitrile are recorded in the range 200–1000 nm. The intense absorption bands at short wavelengths, around 360 nm, may be assigned to ligand to metal ion charge transfer bands (LMCT). The absorptions around 600 nm may be assigned to d–d transitions.

Room temperature magnetic susceptibility measurements for the complexes show that they have magnetic moment values in the range 1.70–1.73 BM, as expected for discrete magnetically non-coupled spin only value for copper(II) ion, as also observed in similar systems.[40]

3.3. Description of the structures

The structures of complexes were confirmed by single crystal X-ray diffraction analysis. The crystallographic and refinement details are summarized in Table S1 (Supplementary

information). Selected bond lengths and bond angles are gathered in Table S2 (Supplementary information).
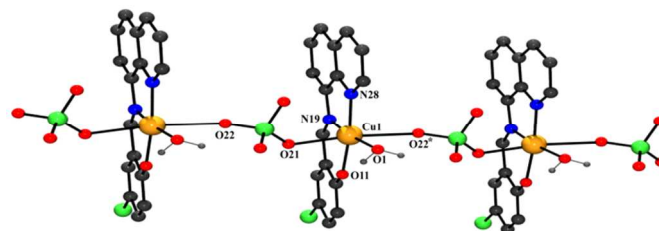

Fig. 1 Perspective view of complex **1** with the selective atom numbering scheme. The hydrogen atoms (except water hydrogen atoms) are not shown for clarity. Symmetry transformation * = 1+x, y, z.

3.3.1. $[Cu(L^1)(H_2O)(OClO_3)]_n$ (1)

The complex **1** crystallizes in the triclinic space group $P\bar{1}$. The structure consists of a 1D infinite chain with the repeating unit $[Cu(L^1)(H_2O)(OClO_3)]^+$ bridged by perchlorate groups (Fig. 1). Within the asymmetric unit, the copper(II) center is six-coordinated, being bonded to nitrogen atoms, N(19), N(28) and a phenoxo oxygen atom, O(11) of the tridentate Schiff base ligand $(L^1)^-$ and an oxygen atom, O(1), of a water molecule in the basal plane. A perchlorate oxygen atom, O(21) and a symmetry related perchlorate oxygen atom, O(22)* (symmetry transformation * = 1+x, y, z) coordinate axially at rather long distances {Cu(1)–O(21) = 2.595(6), Cu(1)–O(22)* = 2.539(6) Å} to form a tetragonally distorted octahedron. The angles and equatorial Cu−N and Cu−O bond lengths of the asymmetric unit, $[Cu(L^1)(H_2O)(OClO_3)]^+$, are in the expected range for typical Jahn−Teller distorted octahedral copper(II) complexes.[41] The shortest copper···copper distance in the polymer is 7.159(2) Å.
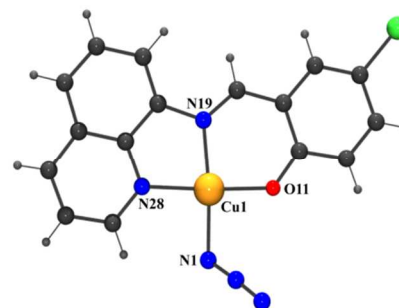

Fig. 2: Perspective view of complex **2** with the selective atom numbering scheme.

3.3.2. $[Cu(L^1)(N_3)]$ (2)

The complex **2** crystallizes in the triclinic space group $P\bar{1}$. A perspective view of the complex together with the atom-numbering scheme is shown in Fig. 2. The structure consists of discrete mononuclear units. The tridentate ligand coordinates to the copper(II) center via the phenolate oxygen atom, O(11), the imine nitrogen atom, N(19), and the pyridinium nitrogen atom, N(28), forming one five member and one six member chelate rings. The azide nitrogen atom, N(1), occupies the fourth

coordination site and completes an ON_3 square plane around the metal center. Sum of the different angles around the copper(II) center is 360.23° indicating almost undistorted square planar geometry around copper(II) center. The trans angles are found to be 175.85(7) {O(11)–Cu(1)–N(28)} and 171.53(8) {N(1)–Cu(1)–N(19)}. Deviations of the coordinating atoms, O(11), N(1), N(19) and N(28), from the least-square mean planes through them are -0.0709(16), 0.070(2), 0.0750(17) and -0.0743(17) Å respectively and that of copper atom from the same plane is -0.0394(2) Å.
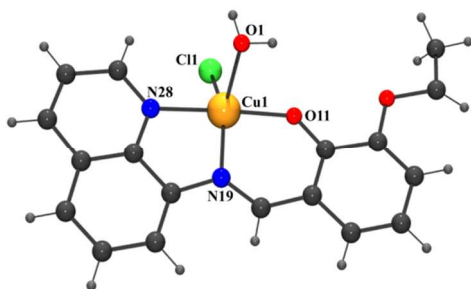

Fig. 3 Perspective view of complex **3** with the selective atom numbering scheme.

3.3.3. *[Cu(L²)(Cl)(H₂O)]* (3)

The complex **3** crystallizes in the monoclinic space group C_2/c. A perspective view of the complex with the atom-numbering scheme is shown in Fig. 3. The tridentate Schiff base ligand, HL^2, coordinates the copper(II) center via the phenolate oxygen atom, O(11), the imine nitrogen atom, N(19) and the pyridinium nitrogen atom, N(28), forming one five member and one six member chelate rings. One water molecule and a chlorine atom coordinate with the copper(II) center forming a square pyramidal structure which is confirmed by the Addison structural index, $\tau = 0.015$ ($\tau = (\alpha - \beta)/60°$, where a and b are the bond angles of the trans donor atoms in the basal plane).[42] The basal plane of the said geometrical structure is formed by two nitrogen donor sites {N(19), N(28)} and one oxygen donor, O(11), from tridentate Schiff base ligand, one chlorine atom, Cl(1) and the apical position is occupied by the oxygen donor, O(1), of a water molecule. Deviations of the coordinating atoms, O(11), N(19), N(28) and Cl(1) from the least-square basal plane are 0.2963(15), -0.3542(17), 0.3218(19) and -0.2638(6) Å, respectively and that of copper atom from the same plane is 0.2847(3) Å. Sum of the different angles around the metal center in the equatorial plane is 360.93°.

3.4. Supramolecular interactions: Theoretical Study

In the polymeric complex **1** we have evaluated energetically the non-covalent interactions that are relevant to rationalize the crystal packing. In particular, the polymeric chains self-assemble by means of π-π stacking and H-bonding interactions involving the extended π-system of the tridentate Schiff base ligand as shown in Fig. 4A. We have used a repeating structural unit of the polymeric chain of complex **1** for the calculations. The theoretical model used to analyze the π-π interaction is shown in Fig. 4B. In the theoretical model we have used only one perchlorate co-ligand to keep the charge of the model neutral (using two perchlorate co-ligands, each monomeric unit would be negatively charged and the interaction repulsive). In addition, the perchlorate ligand of one monomer is located in such a way that does not interact with the organic ligand of the other complex and vice-versa in the theoretical self-assembled dimer (see Fig. 4B). In the X-ray structure, the perchlorate ligands of one polymeric chain interact with the aromatic hydrogen atoms of the organic ligands of the other chain and vice-versa (see dashed lines in Fig. 4A). However, we have used the theoretical dimer shown in Fig. 4B in order to evaluate only the contribution of the weak π-π interaction. Moreover, a close inspection of the π-π complex shows that the chlorine
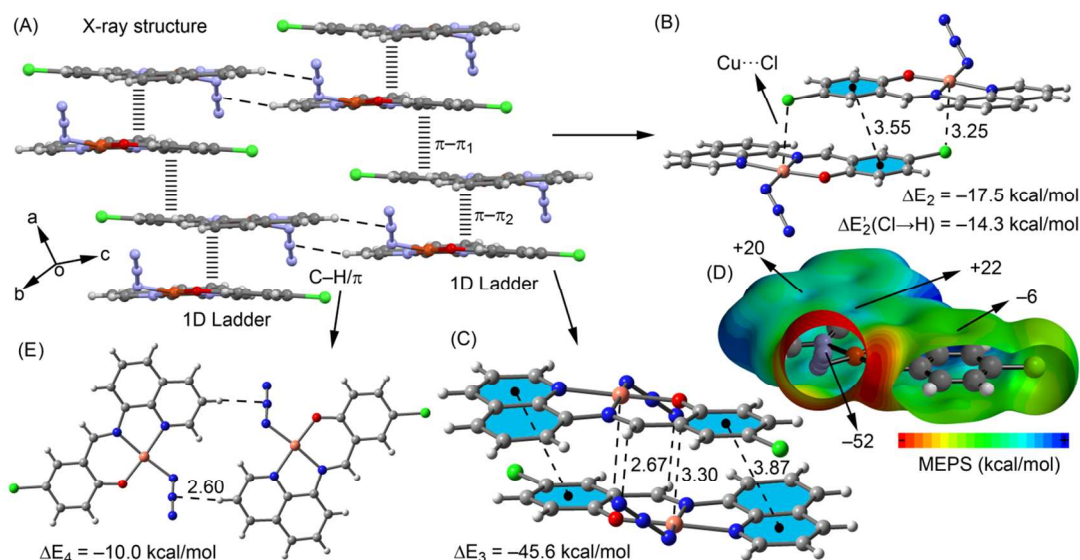

Fig. 5 (A) X-ray fragment of complex **2**. (B, C and E) Theoretical models used to evaluate the non-covalent interactions. (D) Molecular electrostatic surface of complex **2**. Distances are in Å.

atom is close to a C=C bond of the quinoline ring establishing an lp-π interaction. The interaction energy of the self-assembled dimer is large in absolute value ($\Delta E_1 = -17.9$ kcal/mol) and corresponds to two π-π interactions and two lp-π interactions. In order to estimate both contributions separately, we have also computed the interaction energy [denoted as $\Delta E_1'(Cl \to H)$] using a theoretical model where only the chlorine atoms have been replaced by hydrogen atoms and consequently only the stacking interaction is evaluated. As a result the interaction energy is reduced to $\Delta E_1'(Cl \to H) = -14.0$ kcal/mol indicating that each π-π interaction contributes in 7.0 kcal/mol. The difference between both interaction energies correspond to the double lp-π interaction that is weaker than the stacking interaction, i.e. $\Delta E_1 - \Delta E_1'(Cl \to H) = -3.9$ kcal/mol.

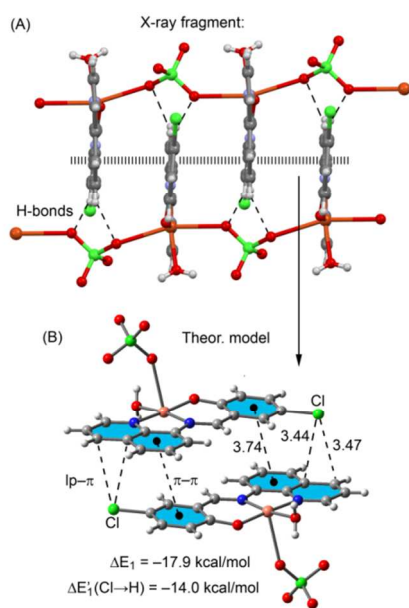**Fig. 4**: (A) X-ray fragment of complex **1**. (B) Theoretical model used to evaluate the lp-π and π-π non-covalent interactions. Distances in Å.

In complex **2** we have evaluated energetically the non-covalent interactions that are significant to explain the assemblies observed in the solid state. In particular, it forms infinite 1D ladders that are dominated by two types of π-π stacking interactions involving the extended π-system of the tridentate Schiff base ligand (see Fig. 5A). This ladder interacts with the adjacent one by means of C–H/π interactions involving the aromatic hydrogen atoms and the π-system of the azide (central N atom). Several non-covalent interactions involving the π-system of coordinated pseudohalides has been analyzed both theoretically and exploring the Cambridge structural database.[43-44] We have used several theoretical models to analyze the π-π and C–H/π interactions that are shown in Fig. 5. Two different π-π stacking modes are observed in the formation of the ladder. The first one (denoted as $\pi\text{-}\pi_1$) is highlighted in the theoretical dimer shown in Fig. 5B. A close inspection of the π-π complex reveals that the chlorine atoms of the ligands establish ancillary interactions with the copper metal centers. The interaction energy of the dimer that represents the $\pi\text{-}\pi_1$ complexation mode ($\Delta E_2 = -17.9$ kcal/mol) is stronger than expected for a π-π stacking due to the presence of both Cu···Cl ancillary interactions. In order to evaluate these ancillary interactions, we have also computed the dimer shown in Fig. 5B where the Cl atoms have been replaced by hydrogen atoms [denoted as $\Delta E_2'(Cl \to H)$] and consequently only the stacking interaction is evaluated. The difference between ΔE_2 and $\Delta E_2'(Cl \to H)$ is the contribution of both Cu···Cl ancillary interactions to the dimer formation, which is -3.2 kcal/mol. The second stacking mode (denoted as $\pi\text{-}\pi_2$), which is also involved in the ladder formation, is highlighted in the dimer shown in Fig. 5C. A close examination shows an intricate combination of interactions in this dimer that include H-bonding, cation-π and π-π interactions. This explains the very large interaction energy computed for this dimer ($\Delta E_3 = -45.6$ kcal/mol), likely due to the electrostatically favoured H-bonding (involving the terminal N atom of azide) and cation-π interactions. To corroborate this, we have computed the molecular electrostatic potential surface (MEPS) of the monomer (see Fig. 5D). It can be clearly
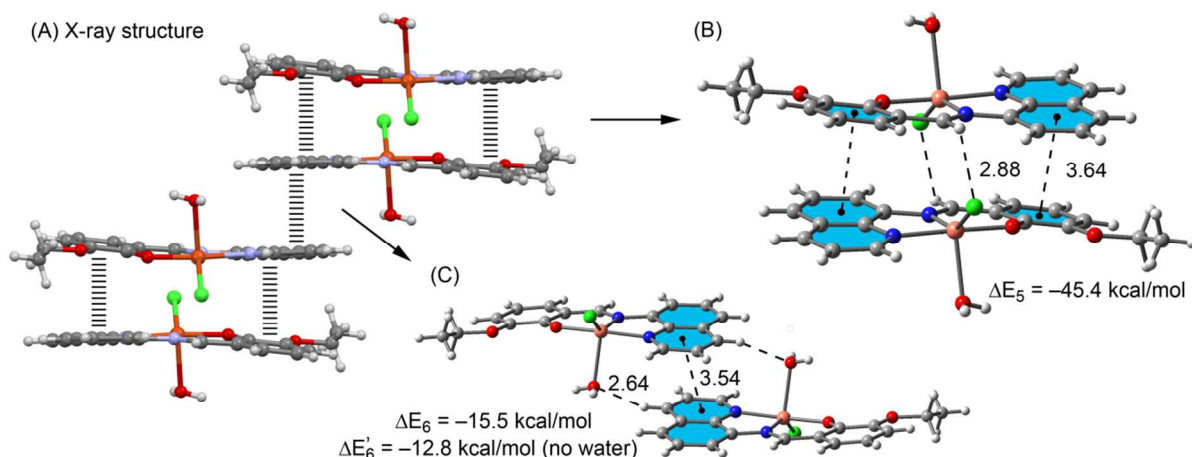

Fig. 6 (A) X-ray fragment of complex **3**. (B and C) Theoretical models used to evaluate the non-covalent interactions. Distances in Å.

observed a region of positive potential over the copper ion (22 kcal/mol) and a region of negative potential (−5 kcal/mol) over the phenolic ring where the cation-π interaction is formed. The 8-aminoquinoline part of the ligand presents a positive potential over the ring and therefore it is not suitable to establish cation-π interactions. The most negative part of the molecule is the ending nitrogen atom of the coordinated azide ligand and the most positive part comprise the aromatic hydrogen atoms thus favouring the H-bonding interaction, explaining the large interaction energy observed in this π-$π_2$ interaction mode and contributing to the stabilization of the 1D ladder observed in the solid state. Finally, we have also computed the interaction energy of both symmetrically related C–H/π(azide) contacts that are responsible for the inter-ladder interaction using the model represented in Fig. 5E. As a result, the interaction energy is $\Delta E_4 = -10.0$ kcal/mol, thus each C–H/π interaction is ½×ΔE_4 = −5.0 kcal/mol, comparable to conventional H-bonding interactions.

In complex **3** we have also analyzed theoretically the non-covalent interactions that are responsible for the formation of the infinite 1D ladder in the solid state that is dominated by two types of π-π stacking interactions (see Fig. 6A). The first one is shown in Fig. 6B and, additionally to the π-π stacking interaction between the electron rich and electron poor rings of the ligand (phenol and quinoline respectively), two strong H-bonds (electrostatically favoured) contribute to the large binding energy computed for this dimer ($\Delta E_5 = -45.4$ kcal/mol). The second one is shown in Fig. 6B and it is characterized by an antiparallel stacking of the coordinated quinoline moieties and two H-bonds involving the coordinated water molecules. The interaction energy of this dimer is $\Delta E_6 = -15.5$ kcal/mol that correspond to both the π-π stacking and H-bonding interactions. We have also computed the interaction energy (denoted as $\Delta E_6'$, see Fig. 6B) of an additional theoretical model where the copper-coordinated water molecules have been eliminated and, consequently, the H-bonds are not established. As a result the interaction energy is reduced to $\Delta E_6' = -12.8$ kcal/mol, that is the contribution of the antiparallel stacking interaction.

3.5. Hirshfeld surface analysis

The Hirshfeld surface[45] surrounded a molecule is defined by points where the attempt to the electron density from the molecule of interest is equal to the contribution from all the other molecules. For each point on that isosurface two distances are determined: one is de represents the distance from the point to the nearest nucleus external to the surface and second one is di represents the distance to the nearest nucleus internal to the surface. The normalized contact distance (d_{norm}) is based on both d_e and d_i. The Hirshfeld surfaces mapped over d_{norm} (range of -0.1–1.5 Å) are displayed in Fig. 7. The Hirshfeld surfaces mapped over shape index and curvedness (range of -0.1–1.5 Å) are shown in Fig. S1-S2 (Supplementary information). The surfaces are shown as transparent to allow visualization of molecules, around which they were calculated. The surface represents the circular depressions (deep red) visible on the

Hirshfeld surface indicative of O···H, Cl···H, N···H contacts. Other visible spots in the Hirshfeld surfaces correspond to H···H contacts. The dominant interactions are seen in d_{norm} surface plots as the bright red areas in Fig. 7. The curvedness surface indicates the electron density surface curves around the molecular interactions. The 2D fingerprint plots of complexes illustrate the significant differences between the intermolecular interaction patterns. In fingerprint plots (Fig. 8, 9 and 10), O···H, Cl···H and N···H interactions are represented by a spike in the bottom area whereas the H···O, H···Cl, H···N interactions are represented by a spike in the top left regions.
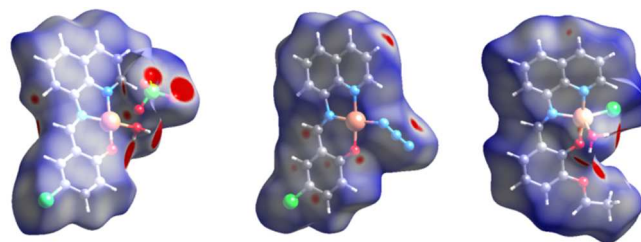

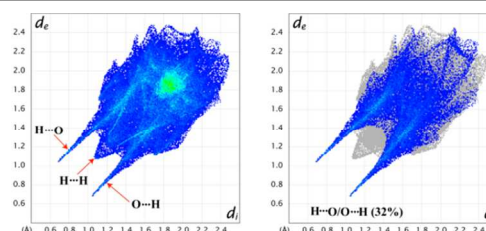**Fig. 7**: Hirshfeld surfaces mapped over d_{norm} for complexes **1** (left), **2** (middle) and **3** (right).

Fig. 8 Fingerprint plots of **1**: full (left) and resolved into H···O/O···H (bottom) contacts showing the percentage of contact contributed to the total Hirshfeld surface area of the molecule.

The proportions of H···O/O···H interactions comprise 32%, 3.5% and 9.6% of the Hirshfeld surfaces for each molecule of **1**, **2** and **3**, respectively. The O···H interaction is represented by a spike ($d_i = 1.067$, $d_e = 0.667$ Å in **1**, di = 1.41, $d_e = 1.07$ Å in **2** and $d_i = 1.233$, de = 0.898 Å in **3**) in the bottom left (donor) area of the fingerprint plot (Fig. 8-10). The H···O interaction is also represented by another spike ($d_e = 1.067$, $d_i = 0.667$ Å in **1**, $d_e = 1.41$, $d_i = 1.07$ Å in **2** and $d_e = 1.233$, $d_i = 0.898$ Å in **3**) in the bottom right (acceptor) region of the fingerprint plot. The proportions of H···Cl/Cl···H interactions comprise 11.6% and 13.6% of the Hirshfeld surfaces for each molecule of complexes **2** and **3**, respectively. The Cl···H interaction is represented by a spike ($d_i = 1.813$, $d_e = 1.167$ Å in **2** and $d_i = 1.367$, $d_e = 0.767$ Å in **3**) in the bottom left (donor) area of the fingerprint plot (Fig. 9-10). The H···Cl interaction is also represented by another spike ($d_e = 1.813$, $d_i = 1.167$ Å in **2** and $d_e = 1.367$, $d_i = 0.767$ Å in **3**) in the bottom right (acceptor) region of the fingerprint plot. The proportion of H···N/N···H interaction comprises 26.4% of the Hirshfeld surfaces for complex **2**. The N···H interaction is represented by a spike ($d_i = 1.433$, $d_e = 1.0$ Å in **2**) in the bottom left (donor) area of the fingerprint plot (Fig. 9). The H···N interaction is represented by

another spike (d_e = 1.433, d_i = 1.0 Å in **2**) in the bottom right (acceptor) region of the fingerprint plot.
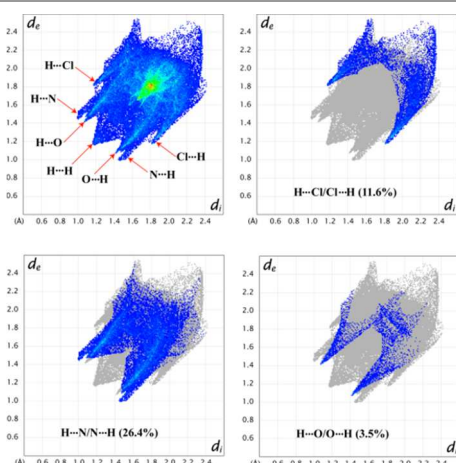
Fig. 9 Fingerprint plots of **2**: full (top left) and resolved into H···Cl/Cl···H (top right), H···N/N···H (bottom left) and H···O/O···H (bottom right) contacts showing the percentage of contact contributed to the total Hirshfeld surface area of the molecule.
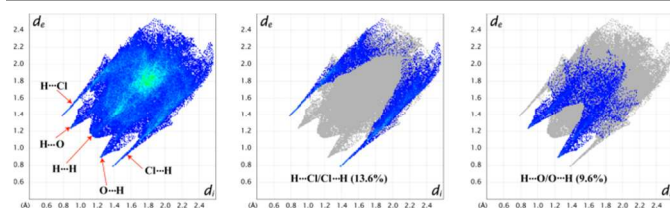
Fig. 10 Fingerprint plots of **3**: full (left) and resolved into H···Cl/Cl···H (middle) and H···O/O···H (right) contacts showing the percentage of contact contributed to the total Hirshfeld surface area of the molecule.

Conclusions

We have synthesized and X-ray characterized three new copper(II) complexes that present interesting supramolecular assemblies in the solid state, which are dominated by H-bonding, π-π and lp-π interactions. Hirshfeld surface analysis was used for visually analyzing intermolecular interactions in the crystal structures. Surfaces mapped with d_{norm} help to envisage hydrogen bonding interactions. Fingerprint plots reveal the percentage of intermolecular contacts (H···H O···H, Cl···H and N···H) in the complexes. On the other hand, we have evaluated energetically, by means of DFT calculations, the contribution of each interaction to the formation of the supramolecular assemblies. The energetic analysis confirms the importance of non-covalent interactions involving π-system of the aromatic ligands.

Acknowledgements

Notes and references

*a*Department of Chemistry, Inorganic Section, Jadavpur University, Kolkata -700 032, India. e-mail: shouvik.chem@gmail.com Tel:+(91)33-24572941.
*b*Departament de Química, Universitat de les IllesBalears, Crta. deValldemossa km 7.5, 07122 Palma (Baleares), Spain. E-mail: toni.frontera@uib.es.
† CCDC 1053588-1053590 for **1**–**3** respectively.

1   P. Kar, R. Biswas, M. G. B. Drew, A. Frontera and Ashutosh Ghosh, *Inorg. Chem.*, 2012, **51**, 1837.
2   P. Manna, S. K. Seth, A. Das, J. Hemming, R. Prendergast, M. Helliwell, S. R. Choudhury, A. Frontera and S. Mukhopadhyay, *Inorg. Chem.*, 2012, **51**, 3557.
3   M. E. S. Moussa, K. Guillois, W. Shen, R. Réau, J. Crassous and C. Lescop, *Chem. Eur. J.*, 2014, **20**, 14853.
4   T. Samanta, L. Dey, J. Dinda, S. K. Chattopadhyay and S. K. Seth, *J. Mol. Struct.*, 2014, **1068**, 58.
5   A. K. Chaudhari, A. Sharma, S. Mukherjee, B. Joarder and S. K. Ghosh, *CrystEngComm*, 2014, **16**, 4691.
6   L. M. Salonen, M. Ellermann and F. Diederich, *Angew. Chem. Int. Ed.*,2011, **50**, 4808.
7   H. J. Schneider, *Angew. Chem., Int. Ed.*, 2009, **48**, 3924.
8   Y.-S. Yang, Y.-P. Yang, M. Liu, Q.-M. Qiu, Q.-H. Jin, J.-J. Sun, H. Chen, Y.-C. Dai and Q.-X. Meng, *Polyhedron*, 2015, 85, 912.
9   Y. Shen, N. Ma, L. Wu and H. –H. Song, *Inorg. Chim.Acta*, 2015, **429**, 51.
10 A. Bhattacharyya, P. K. Bhaumik, P. P. Jana and S. Chattopadhyay, *Polyhedron*, 2014, **78**, 40.
11 S. Carboni, C. Gennari, L. Pignataro and Umberto Piarulli, *Dalton Trans.*, 2011, **40**, 4355.
12 C.-Y. Huang, J. Wang, Z. -Y. Ding and K. Cui, *J. Mol. Struct.*,2015, **1086**, 118.
13 S. Yamada, N. Sako, M. Okuda and A. Hozumi, *CrystEngComm*, 2013, **15**, 199.
14 A. Sasmal, A. Bauzá, A. Frontera, C. Rizzoli, C. Desplanches, L. J. Charbonnièree and S. Mitra, *Dalton Trans.*, 2014, **43**, 6195.
15 I. Caracelli, I. Haiduc, J. Z.-Schpector and E. R.T. Tiekink, *Coord. Chem. Rev.*, 2013, **257**, 2863.
16 F. Orvay, A. Bauzá, M. B.-Oliver, A. G.-Raso, J. J. Fiol, A. Costa, E. Molins, I. Mata and A. Frontera, *CrystEngComm*, 2014, **16**, 9043.
17 L. M. Salonen, M. Ellermann and F. Diederich, *Angew. Chem., Int. Ed.*, 2011, **50**, 4808.
18 D. Paolantoni, J. R.-Magnieto, S. Cantel, J. Martinez, P. Dumy, M. Surin and S. Ulrich, *Chem. Commun.*, 2014, **50**, 14257.
19 C. Estarellas, A. Frontera, D. Quiæonero and P. M. Deyà, *Angew. Chem. Int. Ed.*, 2011, **50**, 415.
20 S. Grimme, *Chem. Eur. J.*, 2012, **18**, 9955.
21 J. L. Atwood, J. W. Steed, Supramolecular Chemistry. Wiley, 2009.
22 A. Hazari, L. K. Das, A. Bauza, A. Frontera and A. Ghosh, *Dalton Trans.*, 2014, **43**, 8007.
23 P. Seth, A. Bauza, A. Frontera and A. Ghosh, *Inorg. Chem. Commun.*, 2014, **41**, 1.

24 A. Bhattacharyya, P. K. Bhaumik, A. Bauza, P. P. Jana, A. Frontera, M. G. B. Drew and S. Chattopadhyay, *RSC Adv.*, 2014, **4**, 58643.

25 H. S. Jena, *RSC Adv.*, 2014, **4**, 3028.

26 H. S. Jena, *Inorg. Chim. Acta*, 2014, **410**, 156.

27 S. Naiya, M. G.B. Drew, C. Estarellas, A. Frontera and A. Ghosh, *Inorg. Chim. Acta*, 2010, **363**, 3904.

28 C. M.-García, A. Bauzá, G. Schnakenburg, A. Frontera and R. Streubel,*CrystEngComm*, 2015, **17**, 1769.

29 O. Kahn, Molecular magnetism; VCH, New York, 1993.

30 G. M. Sheldrick, *ActaCryst.*, 2008, **A64**, 112.

31 G.M. Sheldrick, SADABS: Software for Empirical Absorption Correction, University of Gottingen, Institute furAnorganischeChemiederUniversitat, Gottingen, Germany, 1999–2003.

32 R. Ahlrichs, M. Bär, M. Haser, H. Horn and C. Kölmel, *Chem. Phys. Lett.*, 1989, **162**, 165.

33 S. F. Boys and F. Bernardi, *Mol. Phys.*, 1970, **19**, 553.

34 R. F. W. Bader, *Chem. Rev.*, 1991, **91**, 893.

35 AIMAll (Version 13.11.04), T. A. Keith, TK Gristmill Software, Overland Park KS, USA 2013.

36 S. Roy, P. K. Bhaumik, K. Harms and S. Chattopadhyay, *Polyhedron*, 2014, **75**, 57.

37 M. Mishra, K. Tiwari, P. Mourya, M. M. Singh and V. P. Singh, *Polyhedron*, 2015, **89**, 29.

38 R. Prabu, A. Vijayaraj, R. Suresh, R. Senbhagaraman, V. Kaviyarasan and V. Narayanan, *J. Coord. Chem.*, 2013, 66, 206.

39 Y. -H. Luo, D. -E. Wu, S. -W. Ge, Y. Li and B. -W. Sun, *RSC Adv.*,2014, **4**, 11698.

40 P. Bhowmik, S. Chattopadhyay, M. G. B. Drew and A. Ghosh, *Inorg. Chim. Acta*, 2013, **395**, 24.

41 M. Joas, T. M. Klapötke, J. Stierstorfer and N. Szimhardt, *Chem.-Eur. J.*, 2013, **19**, 9995.

42 A. W. Addison, T. N. Rao, J. Reedijk, J. V. Rijn and G. C. Verschoor, *J. Chem. Soc., Dalton Trans.*, 1984, 1349.

43 A. Hazari, L. K. Das, R. M.Kadam, A.Bauza, A.Frontera and A. Ghosh *Dalton Trans.*, 2015, **44**, 3862.

44 A.Hazari, L. K. Das, A.Bauzá, A.Frontera and A. Ghosh, *Dalton Trans.*, 2014, **43**, 8007.

45 T. Samanta, L. Dey, J. Dinda, S. K. Chattopadhyay and S. K. Seth, *J. Mol. Struct.*, 2014, **1068**, 58.